Challenges and Issues of Modern Science
2026, Vol. 5, No. 1, ID 343
ISSN: 3083-5704
URL: https://cims.fti.dp.ua/j/article/view/343
DOI: https://doi.org/10.15421/cims.5.343

UDC 624.15:624.138.2

Finite Element Analysis of Geogrid Behavior Under a Strip Footing

Brige Dublin Boussa Elenga, Severin Jean Maixent Loubouth

Purpose. This paper presents a two-dimensional finite element analysis (FEA) aimed at evaluating the effectiveness of multi-layer geogrid reinforcement under a strip footing on clayey and sandy soils. The research quantifies the impact of vertical spacing (h) on bearing capacity, settlement reduction, and stress distribution. **Design / Method / Approach.** The FEA methodology utilized the Mohr-Coulomb model and interface elements to simulate soil-geogrid interaction. Simulations were performed using Plaxis 2D, with the depth of the first geogrid layer fixed at u = 0.33B, while the vertical spacing ratio (h/B) ranged from 0.1 to 0.5, keeping other geometric parameters constant. **Findings.** The results confirmed the overall effectiveness of the reinforcement, leading to a significant increase in ultimate bearing capacity and a substantial reduction in settlement compared to unreinforced soil. The analysis identified distinct optimal spacings of h/B = 0.3 for clayey soil and h/B = 0.2 for sandy soil. **Theoretical Implications.** This research validates the role of geogrids as rigid barriers that modify failure surface trajectories. It provides a detailed understanding of load transfer mechanisms by identifying unique tensile signatures: a “bell-shaped” distribution for clay and an "M-shaped" distribution for sand. **Practical Implications.** These findings provide concrete design charts, allowing practitioners to optimize the vertical layout of reinforcement layers to ensure maximum efficiency without material waste. **Originality.** The originality and value of this work lie in the direct and simultaneous comparison of two contrasting soil types under identical geometric configurations, offering a comprehensive perspective on the influence of lithology on geogrid reinforcement. **Research Limitations.** However, the study has limitations, notably its purely numerical and two-dimensional nature, which restricts direct extrapolation to square or circular footing configurations. **Future Research.** Future studies would benefit from incorporating laboratory experimental tests to calibrate the numerical models. **Article type.** Applied Research.

Keywords:

geosynthetic reinforcement, soil-geogrid interaction, multi-layer geogrid, shallow foundation, geogrid vertical spacing, failure mechanism

---

Мета. У статті представлено двовимірний аналіз методом кінцевих елементів (FEA), спрямований на оцінку ефективності багатошарового армування геосіткою стрічкового фундаменту на глинистих і піщаних ґрунтах. Дослідження кількісно визначає вплив вертикального кроку (h) на несучу здатність, зменшення осідання та розподіл напружень. **Дизайн / Метод / Підхід**. Методологія FEA використовувала модель Мора-Кулона та контактні елементи для моделювання взаємодії ґрунту з геосіткою. Моделювання виконувалося в Plaxis 2D, при цьому глибина закладання першого шару геосітки була зафіксована на рівні u = 0.33B, тоді як співвідношення вертикального кроку (h/B) варіювалося від 0.1 до 0.5 за незмінних інших геометричних параметрів. **Результати**. Результати підтвердили загальну ефективність армування, що привело до суттєвого збільшення граничної несучої здатності та значного зменшення осідання порівняно з неармованим ґрунтом. Аналіз виявив відмінні оптимальні значення кроку h/B = 0.3 для глинистого ґрунту та h/B = 0.2 для піщаного ґрунту. **Теоретичне значення**. Дослідження підтверджує роль геосіток як жорстких бар'єрів, що змінюють траєкторії поверхні руйнування. Воно надає детальне розуміння механізмів передачі навантаження шляхом виявлення характерних епюр розтягувальних зусиль: «дзвоноподібного» розподілу для глини та «М-подібного» розподілу для піску. **Практичне значення**. Отримані результати надають конкретні розрахункові діаграми, що дозволяють фахівцям-практикам оптимізувати вертикальне розташування шарів армування для забезпечення максимальної ефективності без надмірних витрат матеріалу. **Оригінальність / Цінність**. Оригінальність і цінність цієї роботи полягають у прямому й одночасному порівнянні двох контрастних типів ґрунту за ідентичних геометричних конфігурацій, що дає комплексне уявлення про вплив літології на армування геосіткою. **Обмеження дослідження / Майбутні дослідження**. Дослідження має обмеження, зокрема виключно числовий і двовимірний характер, що обмежує пряме поширення результатів на квадратні чи круглі конфігурації фундаментів. Подальші дослідження виграли б від включення лабораторних експериментальних випробувань для калібрування числових моделей. **Тип статті**. Прикладне дослідження.

Ключові слова:

геосинтетичне армування, взаємодія ґрунту з геосіткою, багатошарова геосітка, фундамент неглибокого закладання, вертикальний крок геосітки, механізм руйнування

Contributor Details:

Brige Dublin Boussa Elenga, Dr. Sc., Marien Ngouabi University: Brazzaville, Brazzaville, CG & Institut Polytechnique de Kintélé: Kintélé, Brazzaville, CG, dublinbrige@gmail.com
Severin Jean Maixent Loubouth, Dr. Sc., Marien Ngouabi University: Brazzaville, Brazzaville, CG, beniloubouth@gmail.com

Received: 2026-05-07 *Revised: 2026-06-16* *Accepted: 2026-06-17* *Published: 2026-06-28*

Rapid urbanization and the increasing development of transport and energy infrastructure are compelling engineers to construct structures on sites with geotechnical characteristics deemed poor or even unsuitable. These sites, primarily composed of compressible soils or loose deposits, possess insufficient intrinsic mechanical properties to support the loads transmitted by conventional shallow foundations. In this context, the risks of failure by general shear or punching (Gupta et al., 2017; Pham, & Ohtsuka, 2021), as well as the occurrence of excessive differential settlements (Jewell, 1996), constitute major threats to the structural integrity of buildings and the functionality of infrastructure. The prohibitive cost of deep foundations (piles, barrettes) in certain economic contexts drives research toward more agile and sustainable soil improvement solutions.

Among in situ reinforcement techniques, the use of high-tenacity synthetic geogrids has emerged as a preferred alternative, combining economic viability with structural efficiency (Basudhar et al., 2007; El Sawwaf, 2007; Alamshahi & Hataf, 2009). The incorporation of these layers beneath the base of strip footings radically alters the rheological behavior of the soil mass by creating a soil-reinforcement composite with increased stiffness. Historically, the understanding of these systems has evolved since the seminal works of Terzaghi (1943), Meyerhof (1974), and Binquet and Lee (1975), who laid the groundwork for the bearing capacity analysis of reinforced soils by identifying three potential failure modes: reinforcement tension failure, interface sliding, and pull-out failure. However, these initial models, while foundational, relied on simplified stress distribution assumptions that struggle to capture the complexity of the soil-inclusion-structure interaction as it truly manifests under eccentric loads or on heterogeneous soils.

The state of the art has been considerably enriched over recent decades through rigorous experimental, analytical, and numerical investigations (Omar et al., 1993; Tsukada et al., 1993; Khing et al., 1994; Bergado et al., 2002; Ahmad, 2022; Banu et al., 2024). The works of Akinmusuru et al. (1981), Abdel-Baki et al. (1993), Yetimoglu et al. (1994), Dash et al. (2001), Hamidi et al. (2019), Xu et al. (2019) were decisive in demonstrating that reinforcement efficiency depends not only on the intrinsic strength of the geogrid but also on its geometric configuration within the soil mass. Specifically, they highlighted the pivotal role of the first layer depth (u) and inter-layer spacing (h), suggesting the existence of an optimal influence zone beyond which the contribution of the reinforcement becomes marginal. Parallelly, Dash et al. (2003) demonstrated that in cohesive soils, performance is primarily governed by interface adhesion, thereby limiting the lateral displacements of the clayey matrix.

However, despite these advances, a "gray area" persists regarding the coupled response of the system at limit states. Most previous studies have focused either on the increase in ultimate load (ULS) or on the reduction of settlements (SLS), without systematically isolating the influence of vertical spacing variations on these two indicators in a comparative manner across different lithofacies. Furthermore, visualizing internal forces and understanding mobilization mechanisms — whether through lateral confinement or the tensioned membrane effect — remains difficult to grasp through laboratory testing alone.

The present study proposes to fill this knowledge gap through a systematic numerical investigation conducted via the Plaxis 2D finite element software. The originality of this work lies in the rigorous isolation of the impact of vertical spacing (h/B) on two key performance indicators: the Bearing Capacity Ratio (BCR) and the Settlement Reduction Ratio (SR). Through a detailed comparative analysis between sand and clay, this research explores variations in failure kinematics and the mobilization of tensile forces. Ultimately, the objective is to propose optimized design criteria capable of guaranteeing both safety against failure and operational serviceability through deformation control.

Methodology

The numerical methodology adopted to model the complex interaction between the strip footing, the foundation soil, and the geogrids is structured into three (03) stages.

Definition of the Geometric Model. In this study, the geometric model is defined as follows.

– Strip footing: Width B = 2 m, length l = 12 m, and embedment depth Df = 0.

– Geogrid: Width b = B.

– Analysis domain: Height H = 4B and length L = 10B.

Material Properties. To generalize the findings, this study investigates the effect of vertical geogrid spacing variation on both clay and sand. Tables 1, 2, and 3 present the properties of the soil, the geogrid, and the strip footing, respectively.

Table 1 – Geotechnical properties of the soil: Clay and Sand (Source: Developed by the authors)

Properties	Unit	Clay	Sand
Model	-	Mohr-Coulomb	Mohr-Coulomb
Behavior type	-	Drained	Drained
Dry unit weight	kN/m³	16.04	17.13
Satured unit weigh	kN/m³	18.22	20.00
Young's modulus	kN/m²	12100	28500
Poisson's ratio	-	0.33	0.3
Cohesion	kN/m²	5	1
Friction angle	Degree	25	32
Dilatancy angle	Degree	0	3

Table 2 – Properties of the geogrids (Source: Developed by the authors)

Properties	Unit	Geogrid
Behavior type	-	Elastic
Axial stiffness (EA)	kN/m	2100

Table 3 – Properties of the strip footing (Source: Developed by the authors)

Properties	Unit	Strip footing
Axial stiffness (EA)	kN/m	12.23 x 10^6
Flexural rigidity (EI)	kN.m²/m	256.91 x 10^3
Thickness	m	0.502
Self-weight	kN/m/m	12
Poisson's ratio	-	0.17

Numerical Modeling. The numerical modeling of the system was conducted in three (03) successive steps. The first step consisted of constructing the overall geometry, including the soil mass, the strip footing, and the three (03) geogrid layers. The interfaces between the soil and the reinforcements were characterized by an interaction coefficient R_{inter} fixed at 0.7 for clay and 0.82 for sand, to simulate interface adhesion and friction.

The second step was dedicated to the generation of a very fine-type mesh and the establishment of initial soil stresses under its self-weight (geostatic state).The third and final step corresponded to the construction phase, during which the strip footing and geogrids were activated, followed by a vertical loading of 800 kPa.

For each soil type, a reference simulation on unreinforced soil (soil without geogrids) was first carried out. Then, the study of the reinforcement was performed by fixing the depth of the first geogrid layer at u/B = 0.33, while varying the vertical spacing h between layers according to h/B ratios ranging from 0.1 to 0.5.

Following this modeling, the following parameters were calculated:

$$BCR = \frac{\text{Ultimate bearing capacity of the reinforced soil}}{\text{Ultimate bearing capacity of the unreinforced soil}}; \quad (1)$$

$$BCR \text{ discrepancy } (\%) = \frac{|BCR_{Fine} - BCR_{Very\ Fine}|}{BCR_{Very\ Fine}} X100; \quad (2)$$

$$SR = \frac{\text{Settlement of the reinforced soil under a specific load}}{\text{Settlement of the unreinforced soil under the same load}}; \quad (3)$$

$$\text{Settlement Reduction } (\%) = (1 - \text{SR})\ \text{X100}. \quad (4)$$

Results and Discussion

Load–Settlement Curves

Numerical simulations were used to generate the curves of applied pressure versus vertical footing settlement, as shown in Figure 1. It is observed that all configurations, whether reinforced or unreinforced in the case of clayey soil, as shown in Figure 1(a), exhibit increased initial stiffness, characterized by a steep initial slope. Furthermore, the failure load for reinforced configurations is significantly higher than that of the unreinforced case (Reference). This

observation was also made by Binquet and Lee (1975), and Adams et al. (1997). These authors attribute this behavior to the formation of a composite soil-geogrid mattress that stabilizes the soil mass from the very first load increments.

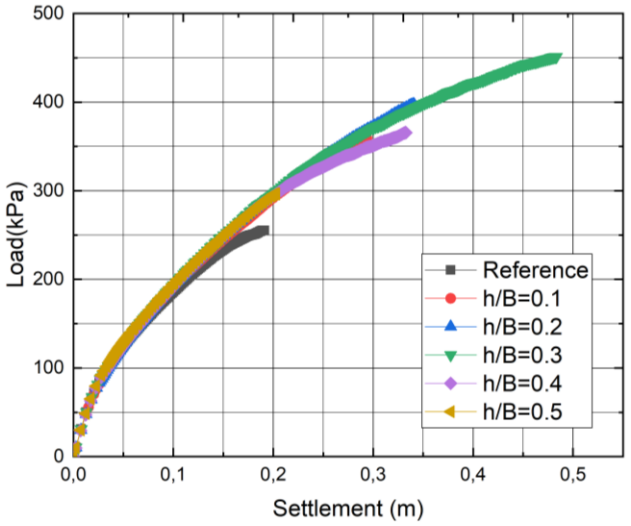

a

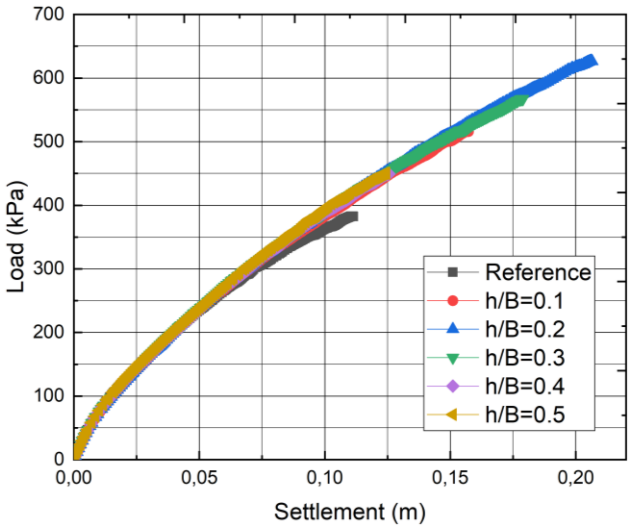

b

Figure 1 – Load-settlement curves for all studied cases: a – Clay soil; b – Sandy soil (Source: Developed by the authors)

In contrast to the clayey soil case shown in Figure 1(a), none of the reinforced or unreinforced configurations for the sandy soil, as shown in Figure 1(b), exhibit this strong initial stiffness. This clearly demonstrates that the system response differs according to the nature of the soil. However, the reinforced configurations achieve, as is the case for the clayey soil, a higher failure load than the unreinforced case (Reference).

Despite this more pronounced difference in initial behavior in the clay, the analysis shows that overall efficiency depends on the reinforcement geometry. While performance is satisfactory for small spacings, it becomes optimal at h = 0.3B for clayey soil and at h = 0.2B for sandy soil. Beyond these values, the interaction between the geogrid layers weakens.

Ultimate Bearing Capacity Improvement

Tables 4 and 5 summarize the data regarding the vertical spacing h between geogrid layers, the ultimate bearing capacity, and the Bearing Capacity Improvement Factor (BCR) for the two (02) studied soil cases (clayey soil and sandy soil). The results obtained reveal the existence of an optimal vertical spacing of h/B = 0.3, with a bearing capacity improvement factor of 1.77 for the clayey soil, while for the sandy soil, it is established at h/B = 0.2, with a bearing capacity improvement factor of 1.63. These values are all greater than 1 and attest to an effective soil reinforcement.

Table 4 – Vertical spacing ratio h/B, ultimate bearing capacity, and Bearing Capacity Ratio (BCR) for clay soil (Source: Developed by the authors)

Vertical spacing ratio h/B	Ultimate bearing Capacity q_u (kPa))	Bearing Capacity Ratio (BCR)
Reference	255.2	
0.1	359.2	1.41
0.2	397.6	1.56
0.3	451.2	1.77
0.4	365.6	1.43
0.5	296.8	1.16

Table 5 – Vertical spacing ratio h/B, ultimate bearing capacity, and Bearing Capacity Ratio (BCR) for sandy soil (Source: Developed by the authors)

Vertical Spacing ratio h/B	Ultimate bearing Capacity q_u (kPa)	Bearing Capacity Ratio (BCR)
Reference	382,4	
0.1	516	1.35
0.2	624,8	1.63
0.3	567,2	1.48
0.4	448,8	1.17
0.5	488	1.17

This improvement in the mechanical behavior of both clay and sandy soils is in perfect alignment with the previous observations of Latha and Somwanshi (2009), who demonstrated that reinforcement efficiency (BCR) is intimately linked to the shear properties of the soil, particularly its internal friction angle. Indeed, although the interaction in the sand (high friction angle) generates significantly higher absolute bearing capacities, the bearing capacity improvement factor (BCR) proves to be higher in the clay (1.77) compared to the sand (1.63). This demonstrates that the relative contribution of the synthetic inclusion is especially pronounced when the initial matrix of the foundation soil exhibits low intrinsic strength.

Furthermore, it is noted that when the spacing h is too small and falls below the optimal spacing, the soil layers between the geogrids are not sufficiently mobilized. Under these conditions, the reinforcement mechanism does not allow the soil to fully develop its shear strength between the geogrid layers, meaning that the additional material is not utilized optimally. Similarly, when the spacing h is too large and exceeds the optimal spacing, the geogrid layers act in isolation without interacting effectively to confine the entire soil mass.

Mesh Sensitivity analysis

The continuous analysis of the data presented in Tables 6 and 7 highlights the existence of complex physical mechanisms and highly non-linear geometric interactions, while definitively validating the numerical stability of the model.

For the clayey soil mass (see Table 6), the optimum reinforcement efficiency remains invariably anchored at a vertical spacing of h/B = 0.3 under the reference Very Fine mesh computing architecture (qu = 451.2 kPa; BCR = 1.77), finding a similar geometric echo in the Fine mesh computations (qu = 527.2 kPa; BCR = 2.06).

Concurrently, for the granular sandy medium (see Table 7), the performance peak remains rigorously fixed at a closer spacing of h/B = 0.2, culminating in a remarkable bearing capacity of 624.8 kPa (BCR = 1.63) under the reference Very Fine discretization, which is validated by the corresponding value obtained with the Fine mesh (qu = 734.4 kPa; BCR = 1.79). This perfect convergence in the spatial location of the improvement peaks attests to the fact that the highlighted interlocking, plastic confinement, and shear failure plane deflection mechanisms reflect a stable rheological reality rather than numerical fluctuations or computational artifacts.

Moreover, the evaluation of the discrepancies demonstrates excellent mathematical convergence, with the difference in BCR exhibiting a moderate value of 9.82% at the optimum of the sandy soil (h/B = 0.2), thereby proving that the numerical model in Plaxis 2D achieves maximum stability when the soil-inclusion interaction operates in perfect kinematic synergy. Outside these optimal operating zones, quantitative divergences emerge due to the specific sensitivity of each lithofacies to local shear gradients. In the clay (cohesive medium), switching from the Very Fine to the Fine mesh in-

duces an artificial stiffening of the model, overestimating the bearing capacity in a non-linear manner. The BCR discrepancy reaches a peak amplitude of 28.48% at h/B = 0.4, before sharply dropping to 0.56% at h/B = 0.5 as the reinforcement group effect completely vanishes. The major conclusion drawn from this comparison thus lies in the absolute invariance of the fundamental qualitative trends with respect to the finite element mesh density employed.

Table 6 – Sensitivity of ultimate bearing capacity to mesh density: Clayey soil (Source: Developed by the authors)

Mesh	Very fine		Fine		
Vertical spacing ratio h/B	Ultimate bearing capacity (kPa)	Bearing Capacity Ratio (BCR)	Ultimate bearing capacity (kPa)	Bearing Capacity Ratio (BCR)	BCR discrepancy (%)
Reference	255.2		256		
0.1	359.2	1.41	388.8	1.52	7.8
0.2	397.6	1.56	439.2	1.72	10.25
0.3	451.2	1.77	527.2	2.06	16.38
0.4	365.6	1.43	471.2	1.84	28.48
0.5	296.8	1.16	299.4	1.17	0.56

Table 7 – Sensitivity of ultimate bearing capacity to mesh density: Sandy soil (Source: Developed by the authors)

Mesh	Very fine		Fine		
Vertical spacing ratio h/B	Ultimate bearing capacity (kPa)	Bearing Capacity Ratio (BCR)	Ultimate bearing capacity (kPa)	Bearing Capacity Ratio (BCR)	BCR discrepancy (%)
Reference	382,4		409.6		
0.1	516	1,35	555.2	1.36	0.74
0.2	624.8	1,63	734.4	1.79	9.82
0.3	567.2	1,48	535.2	1.31	11.49
0.4	448.8	1,17	504.8	1.23	5.13
0.5	488	1,17	462.4	1.13	3.42

Ultimate displacement at failure

Tables 8 and 9 respectively present the ultimate displacements at failure for clay and sandy soils as a function of the spacing between geogrid layers. Overall, a consistent mechanical response is observed for both soil types studied, characterized by a non-linear evolution of performance. For the clayey soil, a growth phase in reinforcement effectiveness is observed until reaching a peak displacement at the optimal spacing of h/B = 0.3, with a maximum value of 0.481 m. Conversely, for the sandy soil, although the trend is substantially identical, the optimum shifts slightly to h/B = 0.2, with a maximum value of 0.205 m. At these specific spacings (0.2 for sand and 0.3 for clay), the soil-reinforcement interaction is most intense, allowing for maximum mobilization of friction forces and optimal confinement of soil particles between the layers.

Table 8 – Ultimate displacement for clayey soil (Source: Developed by the authors)

Vertical spacing ratio h/B	Settlement (m)
Reference	0.191
0.1	0.293
0.2	0.345
0.3	0.481
0.4	0.331
0.5	0.202

Table 9 – Ultimate displacement for sandy soil (Source: Developed by the authors)

Vertical spacing ratio *h*/B	Settlement (m)
Reference	0.111
0.1	0.157
0.2	0.205
0.3	0.179
0.4	0.125
0.5	0.124

A crucial point of this study lies in the behavior of the reference soil (unreinforced), which, under the application of the load, reaches its failure threshold extremely quickly and at a very shallow depth (0.191 m for clayey soil and 0.111 m for sandy soil). This early instability of the natural soil highlights the inability of the unreinforced granular or cohesive structure to dissipate stresses at depth. In contrast, the introduction of geogrids radically modifies this behavior; the reinforced system supports much higher loads while mobilizing greater displacements before failure (moving from the reference case to peaks of 0.481 m or 0.205 m). As highlighted by Latha and Somwanshi (2009), this response reflects a significantly more ductile behavior, where the reinforcement prevents the abrupt failure of the soil mass. This phenomenon demonstrates that the reinforcement delays the appearance of superficial failure mechanisms by redistributing pressures within an expanded "stress bulb." This observation is consistent with the work of Sharma et al. (2009), which demonstrates that the reinforcement forces the failure zone to develop deeper into the foundation soil.

Consequently, beyond the respective optima of 0.2 and 0.3, the decline in performance, which reaches 0.202 m for clayey soil and 0.124 m for sandy soil at h/B = 0.5, reflects a loss of synergy between the reinforcements, thereby gradually bringing the behavior of the soil mass back toward that of an unreinforced soil.

Settlement Reduction

The analysis of Tables 10 and 11, reporting the Settlement Reduction (SR) ratio, allows for the evaluation of reinforcement performance during the service phase. It is observed that for a service load of q = 240 kPa, the maximum settlement reduction rate for the clayey soil is 11.95% at a spacing of h/B = 0.3, compared to 5.88% for sand at h/B = 0.2.

Table 10 – Settlement values, Settlement Efficiency Ratio (SR), and Settlement Reduction Rate for clay soil (Source: Developed by the authors)

Vertical spacing ratio h/B	Settlement (m)	Settlement Efficiency Ratio (SR)	Settlement Reduction (%)
Reference	0.159		
0.1	0.145	0.91	8.81
0.2	0.141	0.89	11.32
0.3	0.14	0.88	11.95
0.4	0.143	0.9	10.06
0.5	0.141	0.89	11.32

Table 11 – Settlement values, Settlement Efficiency Ratio (SR), and Settlement Reduction Rate for sandy soil (Source: Developed by the authors)

Vertical spacing ratio h/B	Settlement (m)	Settlement Efficiency Ratio (SR)	Settlement Reduction (%)
Reference	0.051		
0.1	0.05	0.98	1.96
0.2	0.048	0.94	5.88
0.3	0.05	0.98	1.96
0.4	0.051	1	0
0.5	0.051	0.98	1.96

This significant reduction in settlement confirms that the geogrid acts as a stress-redistributing element, increasing the overall stiffness modulus of the soil mass well before reaching ultimate limit states. This observation aligns with the conclusions of Saha Roy and Deb (2021), who explain that the inclusion of geogrids in-

creases the subgrade reaction modulus, thereby limiting initial elastic deformations.

Furthermore, it is noted that as the spacing increases (h/B > 0.2 or h/B > 0.3), the SR ratio tends toward 1, indicating that the settlement reduction effect fades and the soil mass reverts to a compressibility close to that of natural soil. For the sandy soil, although the SR is also improved, the reduction is less pronounced than in the clay, which is explained by the more compressible nature of the clayey matrix. As highlighted by Huang & Tatsuoka (1990), the effectiveness of reinforcement on settlement control is directly linked to the soil's ability to mobilize confinement stresses; sand, through its interlocking mechanism, offers a stiffer response than clay.

This analysis demonstrates that the optimal spacing is not only a criterion for failure resistance but also a parameter for controlling differential settlements, which are essential for the longevity of structures. Despite this difference in the magnitude of reduction between the two materials, the work of Lovisa et al. (2010) confirms that maintaining a tight vertical spacing is a sine qua non condition for transforming the soil mass into a rigid composite.

Strain and Stress Analysis

Strain Analysis. Figures 2 and 3 illustrate the zones of high shear concentration, outlining the slip surfaces for clay and sandy soils, respectively. For the reference (unreinforced) cases, a curved line is observed starting from the edge of the footing and rising almost instantaneously and superficially toward the surface, indicating shallow failure. This rapid ascent of the shear curve reflects the soil's intrinsic inability to dissipate energy beyond the initial layers beneath the foundation.

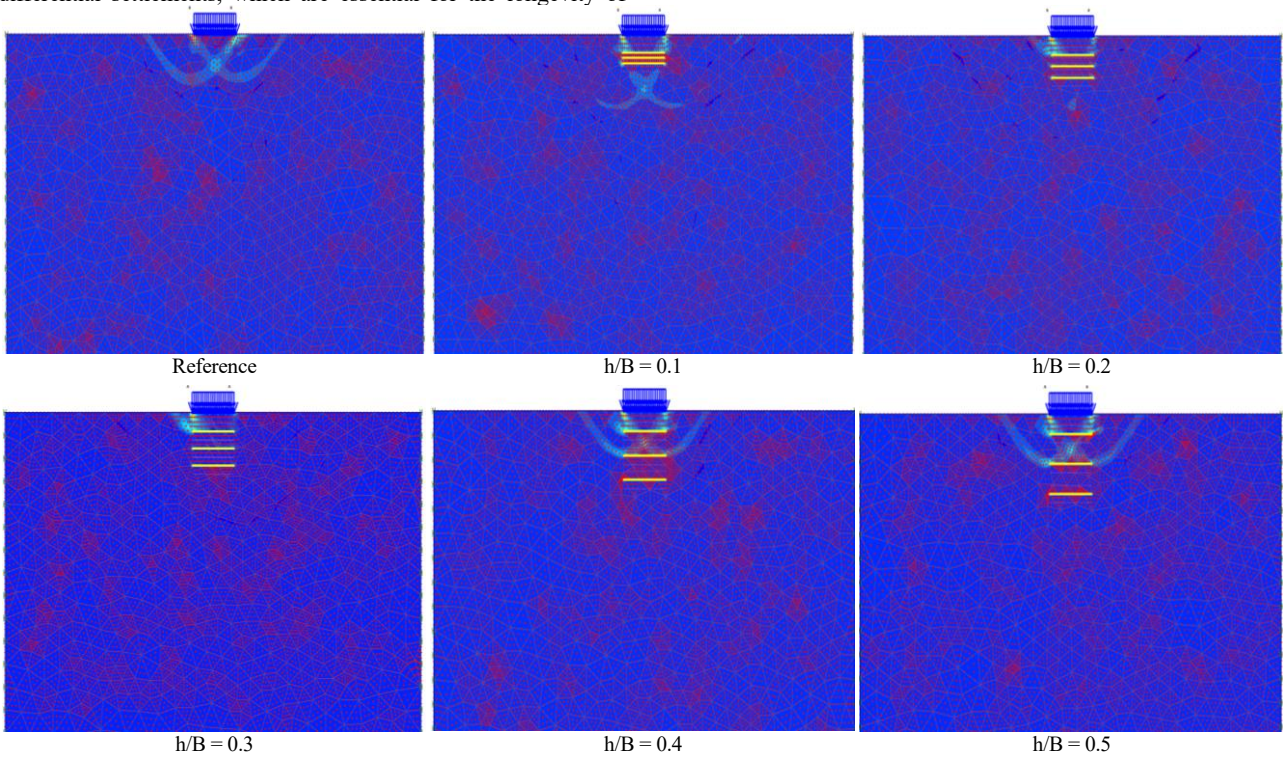

Figure 2 – Geogrid deformations: Clay soil (Source: Developed by the authors)

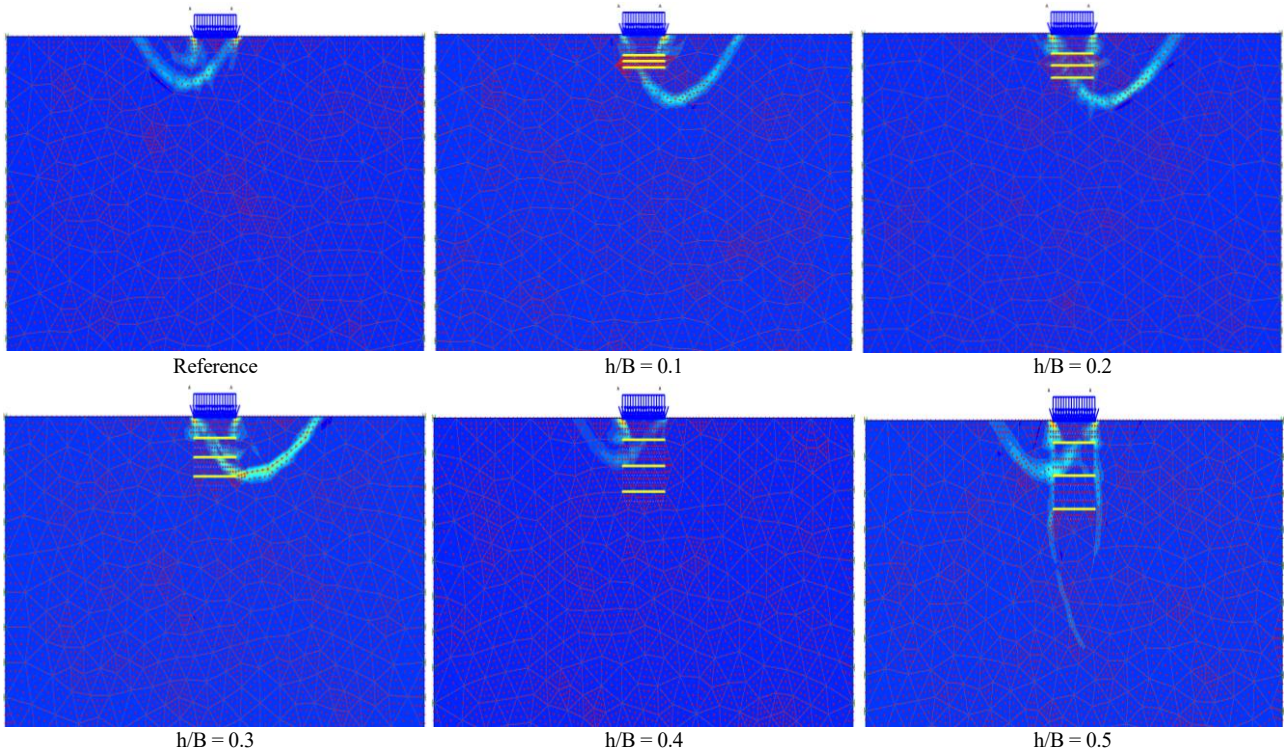

Figure 3 – Geogrid deformations: Sandy soil (Source: Developed by the authors)

In contrast, for the reinforced soils — specifically at h/B = 0.3 and h/B = 0.2 — a radical modification of the failure kinematics is observed. The shear line bypasses the geogrid layers, and the slip surface is shifted deeper, mobilizing a significantly larger volume of soil. This demonstrates that geogrids act as a kinematic barrier. Their introduction into the soil induces a major lateral confinement effect, often referred to as the interlocking effect. This displacement of the failure surface toward deeper layers is a mechanism documented by Boushehrian et al. (2003), who demonstrate that reinforcement prevents the formation of local failure mechanisms by forcing the development of a deeper general failure.

This mechanism operates by restricting the lateral displacement of soil particles located between the reinforcement layers, thereby creating a “pseudo-cohesion” that stiffens the soil mass. This synergy explains why the peak vertical displacement reaches 0.205 m for the sandy soil and 0.481 m for the clayey soil. The geogrid does not merely support the load; it forces the soil to mobilize its resistance over a greater depth, thus expanding the stress bulb. This physically explains the observed increase in the BCR factor. As explained by Zhou and Wen (2008), geogrids act as a "tensioned membrane" that redistributes vertical stresses into horizontal confinement stresses, thereby widening the pressure diffusion zone.

However, the decline in performance observed beyond these optima, which drops to 0.124 m for sandy soil and 0.202 m for clayey soil at h/B = 0.5, suggests the existence of a critical influence zone for each layer. When the spacing exceeds this threshold, the confinement zones no longer overlap, leaving layers of "free" soil that facilitate early failure comparable to that of the reference soil. The relative proximity of the optima for sand and clay tends to demonstrate that, in this geometric configuration, the geogrid's ability to restrain grain movement prevails over variations in the material's internal friction angle.

Stress Analysis. Figures 4(a) and 4(b) illustrate the axial force distribution curves within the geogrids for different spacing cases, respectively for both soil types (clayey and sandy soil). A fundamental distinction is observed based on the nature of the soil, revealing two distinct mechanical signatures. For the clayey soil, all tensile curves across the different spacing cases adopt a “bell-shaped” configuration, characterized by a single peak coinciding with the foundation's axis of symmetry. This shape reflects the predominance of the lateral restraint mechanism. This is explained by the fact that under the vertical load, the cohesive clay matrix undergoes maximum radial expansion beneath the center of the footing, which is intercepted by the interface adhesion of the geogrid. This central distribution is consistent with the work of Palmeira (2009), who demonstrates that in fine-grained soils, tensile mobilization is maximal where the lateral displacement gradient is strongest — namely, under the axis of the load.

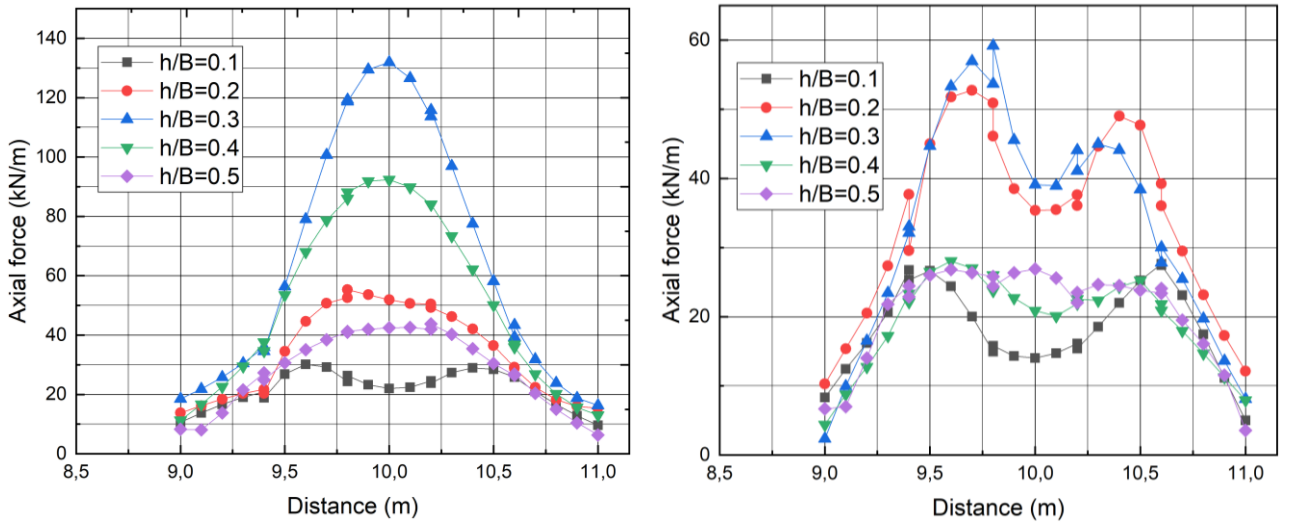

Figure 4 – Distribution curves of axial forces within the geogrids: a – Clay soil; b – Sandy soil (Source: Developed by the authors)

Conversely, the sandy soil exhibits an “M-shaped” distribution, marked by two intensity peaks located directly beneath the edges of the footing, with the most significant occurring at h/B = 0.2. This morphology indicates that the mobilization of the reinforcement is primarily driven by the interception of intense shear zones and by the interlocking effect of granular particles within the geogrid apertures. In this case, the geogrid acts as a direct kinematic barrier at the footing edges, which are critical initiation zones for failure. As observed by Moraci and Gioffrè (2006), this “M” signature reflects the anchoring of reinforcements in lateral passive thrust zones, where the granular soil attempts to escape through the sides of the footing. This more aggressive mobilization of forces at the edges explains the superiority of the Bearing Capacity Ratio (BCR) observed in sand compared to clay, confirming that reinforcement efficiency is intrinsically linked to the inclusion's ability to redistribute shear stresses toward the peripheral zones of the pressure bulb.

Conclusions

The present study aimed to evaluate and compare the effectiveness of geogrid reinforcement for shallow foundations resting on sand and clay soil masses through numerical modeling using Plaxis 2D. The results obtained reveal the following.

Optimal Spacing. There exists a differentiated optimal vertical spacing of h/B = 0.3 for clay and h/B = 0.2 for sand.

Bearing Capacity and Settlement. The introduction of geogrids significantly improves bearing capacity, with the Bearing Capacity Ratio (BCR) reaching 1.63 for sand compared to 1.77 for clay. Simultaneously, the Settlement Reduction (SR) ratio demonstrates that the reinforcement stabilizes the soil mass from the service phases, reducing vertical deformations more markedly in the granular medium.

Kinematic Mechanisms. Geogrids act as a rigid barrier, forcing the slip surface to develop deeper within the soil, thereby mobilizing a passive resistance volume significantly greater than that of unreinforced soil.

Tensile Profiles. The “bell-shaped” tensile profile observed in clay validates a central lateral restraint mechanism, while the "M-shaped" profile identified in sand illustrates an interlocking effect and effective interception of shear zones at the footing edges.

In summary, although reinforcement limits particle displacement in both configurations, the load transfer mechanism differs radically depending on the medium's cohesion. The system transitions from central lateral confinement in clay to a peripheral interlocking mechanism in sand. This work highlights the necessity for refined design approaches, where the choice of reinforcement geometry must be inseparable from the mechanical signature of the foundation soil.

References

Abdel-Baki, S., Raymond G. P, & Jhonson P. (1993). Improvement of the bearing capacity of footings by a single layer of reinforcement. In *Geosynthetic'93 Conf. Proc.* (Vol. 1, pp. 407-416). https://cir.nii.ac.jp/crid/1572824499400383872

Adams, M. T., & Collin, J. G. (1997). Large model spread footing load tests on geosynthetic reinforced soil foundations. *Journal of Geotechnical and Geoenvironmental Engineering, 123*(1), 66–72. https://doi.org/10.1061/(asce)1090-0241(1997)123:1(66)

Ahmad, H. (2022). Sustainability effect of geogrid reinforced tire-shred sand mixtures on the load pressure-settlement response of shallow footing. *Heliyon, 8*(11), e11743. https://doi.org/10.1016/j.heliyon.2022.e11743

Akinmusuru, J. O., & Akinbolade, J. A. (1981). Stability of loaded footings on reinforced soil. *Journal of the Geotechnical Engineering Division, 107*(6), 819–827. https://doi.org/10.1061/ajgeb6.0001153

Alamshahi, S., & Hataf, N. (2009). Bearing capacity of strip footings on sand slopes reinforced with geogrid and grid-anchor. *Geotextiles and Geomembranes, 27*(3), 217–226. https://doi.org/10.1016/j.geotexmem.2008.11.011

Banu, S., Attom, M., Abed, F., Vandanapu, R., Astillo, P. V., Al-Lozi, N., & Khalil, A. (2024). Numerical analysis of the ultimate bearing capacity of strip footing constructed on sand-over-clay sediment. *Buildings, 14*(4), 1164. https://doi.org/10.3390/buildings14041164

Basudhar, P. K., Saha, S., & Deb, K. (2007). Circular footings resting on geotextile-reinforced sand bed. *Geotextiles and Geomembranes, 25*(6), 377–384. https://doi.org/10.1016/j.geotexmem.2006.09.003

Bergado, D. T., Long, P. V., & Srinivasa Murthy, B. R. (2002). A case study of geotextile-reinforced embankment on soft ground. *Geotextiles and Geomembranes, 20*(6), 343–365. https://doi.org/10.1016/s0266-1144(02)00032-8

Binquet, J., & Lee, K. L. (1975). Bearing capacity analysis of reinforced earth slabs. *Journal of the Geotechnical Engineering Division, 101*(12), 1257–1276. https://doi.org/10.1061/ajgeb6.0000220

Boushehrian, J. H., & Hataf, N. (2003). Experimental and numerical investigation of the bearing capacity of model circular and ring footings on reinforced sand. *Geotextiles and Geomembranes, 21*(4), 241-256. https://doi.org/10.1016/s0266-1144(03)00029-3

Dash, S. K., Rajagopal, K., & Krishnaswamy, N. R. (2001). Strip footing on geocell reinforced sand beds with additional planar reinforcement. *Geotextiles and Geomembranes, 19*(8), 529–538. https://doi.org/10.1016/s0266-1144(01)00022-x

Dash, S. K., Sireesh, S., & Sitharam, T. G. (2003). Model studies on circular footing supported on geocell reinforced sand underlain by soft clay. *Geotextiles and Geomembranes, 21*(4), 197–219. https://doi.org/10.1016/s0266-1144(03)00017-7

El Sawwaf, M. A. (2007). Behavior of strip footing on geogrid-reinforced sand over a soft clay slope. *Geotextiles and Geomembranes, 25*(1), 50–60. https://doi.org/10.1016/j.geotexmem.2006.06.001

Gupta, A., Dutta, R. K., Shrivastava, R., & Khatri, V. N. (2017). Ultimate Bearing Capacity of Square/Rectangular Footing on Layered Soil. *Indian Geotechnical Journal, 47*(3), 303–313. https://doi.org/10.1007/s40098-017-0233-y

Hamidi, A., & Abbeche, K. (2019). Bearing capacity of strip footing built on geogrid-reinforced sand over soft clay slope and subjected to a vertical load. *Electronic Journal of Structural Engineering, 19*, 23-32. https://doi.org/10.56748/ejse.19232

Huang, C.-C., & Tatsuoka, F. (1990). Bearing capacity of reinforced horizontal sandy ground. *Geotextiles and Geomembranes, 9*(1), 51–82. https://doi.org/10.1016/0266-1144(90)90005-w

Jewell, R. A. (1996). *Soil reinforcement with geotextiles* (CIRIA Special Publication Vol. 123). Construction Industry Research and Information Association. https://books.google.com/?id=IwFSAAAAMAAJ

Khing, K. H., Das, B. M., Puri, V. K., Yen, S. C., & Cook, E. E. (1994). Foundation on strong sand underlain by weak clay with geogrid at the interface. *Geotextiles and Geomembranes, 13*(3), 199–206. https://doi.org/10.1016/0266-1144(94)90035-3

Latha, G. M., & Somwanshi, A. (2009). Effect of reinforcement form on the bearing capacity of square footings on sand. *Geotextiles and Geomembranes, 27*(6), 409–422. https://doi.org/10.1016/j.geotexmem.2009.03.005

Lovisa, J., Shukla, S. K., & Sivakugan, N. (2010). Behaviour of prestressed geotextile-reinforced sand bed supporting a loaded circular footing. *Geotextiles and Geomembranes, 28*(1), 23–32. https://doi.org/10.1016/j.geotexmem.2009.09.002

Meyerhof, G. G. (1974). Ultimate Bearing Capacity of Footings on Sand Layer Overlying Clay. *Canadian Geotechnical Journal, 11*(2), 223–229. https://doi.org/10.1139/t74-018

Moraci, N., & Gioffrè, D. (2006). A simple method to evaluate the pullout resistance of extruded geogrids embedded in a compacted granular soil. *Geotextiles and Geomembranes, 24*(2), 116–128. https://doi.org/10.1016/j.geotexmem.2005.11.001

Omar, M. T., Das, B. M., Puri, V. K., & Yen, S. C. (1993). Ultimate bearing capacity of shallow foundations on sand with geogrid reinforcement. *Canadian Geotechnical Journal, 30*(3), 545–549. https://doi.org/10.1139/t93-046

Palmeira, E. M. (2009). Soil–geosynthetic interaction: Modelling and analysis. *Geotextiles and Geomembranes, 27*(5), 368–390. https://doi.org/10.1016/j.geotexmem.2009.03.003

Pham, Q. N., & Ohtsuka, S. (2021). Ultimate bearing capacity of rigid footing on two-layered soils of sand–clay. *International Journal of Geomechanics, 21*(7), 04021115. https://doi.org/10.1061/(asce)gm.1943-5622.0002095

Saha Roy, S., & Deb, K. (2021). Modulus of subgrade reaction of unreinforced and geogrid-reinforced granular fill over soft clay. *International Journal of Geomechanics, 21*(9). https://doi.org/10.1061/(asce)gm.1943-5622.0002115

Sharma, R., Chen, Q., Abu-Farsakh, M., & Yoon, S. (2009). Analytical modeling of geogrid reinforced soil foundation. *Geotextiles and Geomembranes, 27*(1), 63–72. https://doi.org/10.1016/j.geotexmem.2008.07.002

Terzaghi, K. (1943). *Theoretical Soil Mechanics*. John Wiley & Sons, Inc. https://doi.org/10.1002/9780470172766

Tsukada, Y., Isoda, T., & Yamanouchi, T. (1993). Geogrid subgrade reinforcement and deep foundation improvement, Yono City, Japan. In *Geosynthetics case histories* (pp. 158–159). BiTech Publishers. https://trid.trb.org/View/413276

Xu, C., Liang, C., & Shen, P. (2019). Experimental and theoretical studies on the ultimate bearing capacity of geogrid-reinforced sand. *Geotextiles and Geomembranes, 47*(3), 417–428. https://doi.org/10.1016/j.geotexmem.2019.01.003

Yetimoglu, T., Wu, J. T. H., & Saglamer, A. (1994). Bearing capacity of rectangular footings on geogrid-reinforced sand. *Journal of Geotechnical Engineering, 120*(12), 2083–2099. https://doi.org/10.1061/(asce)0733-9410(1994)120:12(2083)

Zhou, H., & Wen, X. (2008). Model studies on geogrid- or geocell-reinforced sand cushion on soft soil. *Geotextiles and Geomembranes, 26*(3), 231–238. https://doi.org/10.1016/j.geotexmem.2007.10.002